Applied Surface Science 521 (2020) 145959

Contents lists available at ScienceDirect

Applied Surface Science

journal homepage: www.elsevier.com/locate/apsusc

Full Length Article

Nitric oxide attachment to SPIONs: Demonstration of the covalent S—NO bond in a nanodelivery system

L.K. Mireles[a], D. Stanicki[b], S. Laurent[b], D. Deschênes[c], E. Sacher[a,d], L'H. Yahia[a]

[a] Laboratoire d'Innovation et d'Analyse de Bioperformance, Département de Génie mécanique, École Polytechnique de Montréal, C.P. 6079, Succursale Centre-ville, Montréal, Québec H3C 3A7, Canada
[b] General, Organic and Biomedical Chemistry Unit, Nuclear Magnetic Resonance and Molecular Imaging Laboratory, University of Mons, Avenue Maistriau 19, B7000 Mons, Belgium
[c] Département de Chimie, Université de Montréal, C.P. 6128, Succursale Centre-ville, Montréal, Québec H3C 3J7, Canada
[d] Département de Génie physique, École Polytechnique de Montréal, C.P. 6079, Succursale Centre-ville, Montréal, Québec H3C 3A7, Canada

ARTICLE INFO

Keywords:
Mercaptonitrosation
SPION
Surface analysis

ABSTRACT

We demonstrate the successful functionalization of magnetite (Fe_3O_4) nanoparticles, using PEGdithiol and dimercaptosuccinic acid (DMSA). Following functionalization, TEM images show increased sizes, due to the presence of well-defined polymeric coatings. On subsequent nitrosation, X-ray photoelectron spectroscopy (XPS) and time-of-flight secondary ion mass spectroscopy (TOF-SIMS) show the presence of S—NO bonds.

1. Introduction

Nitric oxide (NO) is a diatomic free radical and endogenous antimicrobial agent, active in many physiological processes. In the human body, it is produced by macrophages, prompted by the immune response to bacterial infection [1]. In 1983, Mancinelli et al. [2] demonstrated its antimicrobial efficacy, destroying colonies of bacteria. Recently, several investigations focused on NO as an effective endogenous molecule against pathogens, due to its antibacterial properties [3,4].

At low concentrations, NO acts as a potent nitrosating agent that promotes the growth and activity of immune cells; at higher concentrations, it alters DNA replication, and regulates protein and cell function, thus inhibiting or killing target pathogens [4,5]. The bacteriostatic and bactericidal properties of NO, and its platelet activation, wound healing and host defense against infections [6–8], suggest that, incorporated as an antimicrobial agent into biomaterials, it would inhibit bacterial growth and, therefore, avoid common infections, such as those induced by *S. aureus*, *E. coli* and others commonly found at hospitals [9–11]. Our ultimate aim is to develop a NO nanodelivery system against biofilms on implant surfaces, based on superparamagnetic iron oxide nanoparticles (SPIONs).

Inorganic nanoparticles have been studied as vehicles for the controlled delivery of drugs such as NO [12,13]. Several of these NO-containing nanoparticle platforms have been synthesized and used specifically for antibiofilm applications, highlighting the feasibility and importance of developing these technologies to prevent contamination of prosthetic devices [14,15].

Currently, the use of SPIONs in the biomedical field is increasing because, when used as nanocarriers, they can be guided to the specific target sites, *in vivo*, by external magnetic fields [16,17]. They possess low cytotoxicity [18] and high biocompatibility [19], and have been approved, by the United States Food and Drug Administration (FDA), as prodrugs for clinical MRI applications [20,21]. *In vivo*, SPIONs are metabolized to ferric ions, which are incorporated into the biological iron storage pool, such as erythrocytes, indicating their acceptable use in humans [22]. Here, magnetite nanoparticles were functionalized by coatings of both dimercaptosuccinic acid (DMSA) and poly (ethylene glycol) dithiol (PEGdithiol); both coatings formed shells containing free thiol (-SH) ligands on the SPION surface, subsequently used as reactive groups for nitrosation, forming mercaptonitroso (S—NO) groups for NO release.

The efficacy of DMSA in drug delivery was previously demonstrated [23], as were its minimal cytotoxic effects [24]. PEG has been widely used as a coating material for magnetic nanoparticles; it is easily metabolized, having nonimmunogenic and nonantigenic properties, and can interact with cell membranes, resulting in an enhanced cellular response [25]. However, it is not biodegradable, and its repeated dosage and accumulation can give rise to accelerated blood clearance. Del Puerto et al. [26], and others [27,28], note that the use of PEG and DMSA, as magnetic nanoparticle coatings, reduces surface charge density, achieves long circulation times and maintains hydrodynamic sizes under 100 nm, avoiding agglomeration.

E-mail address: karina.mireles@polymtl.ca (L.K. Mireles).

https://doi.org/10.1016/j.apsusc.2020.145959
Received 26 June 2019; Received in revised form 5 February 2020; Accepted 2 March 2020
Available online 06 March 2020
0169-4332/

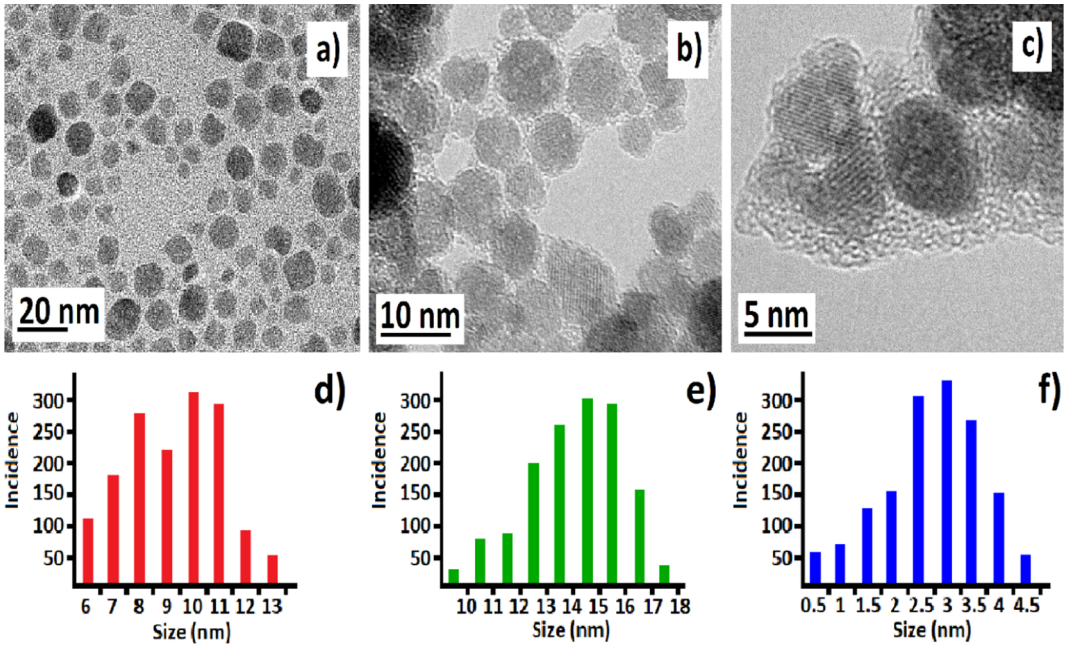

Fig. 1. (a) SPIONs, (b) a thin PEG layer is visible around the SPIONs, (c) PEG thickness is seen to be quite variable. The histogram (d) shows the size distribution of the bare SPIONs; (e) shows the size distribution of the PEGylated SPIONs and (f) shows the size distribution of the PEG layer (2.7 ± 1.3 nm). The length of a PEG dithiol chain, $M_n \sim 1000$, is ~3× the size of the average thickness.

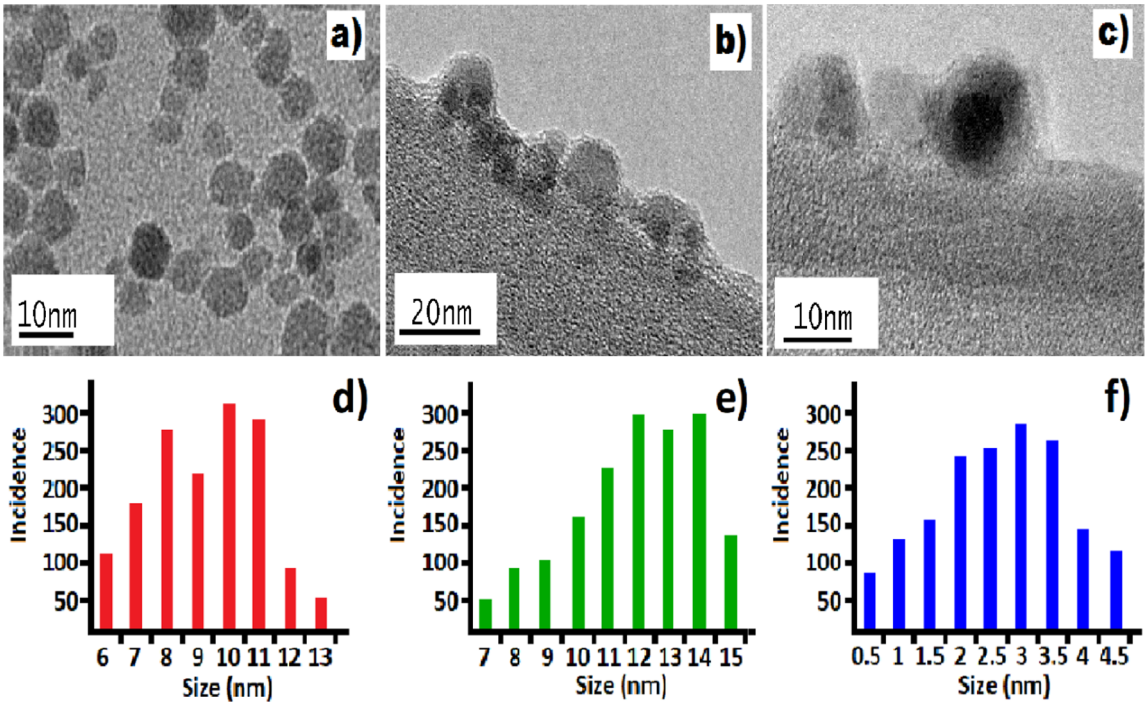

Fig. 2. (a) SPIONs, (b) a thin DMSA layer is visible around the SPIONs, (c) the shell thickness is seen to be quite uniform; average thickness of 3.1 nm ± 1.7 nm. The histogram (d) shows the size distribution of the bare SPIONs; (e) shows the size distribution of the coated SPIONs and (f) shows the size distribution of the DMSA layer (3.1 ± 1.7 nm). The length of a DMSA molecule is about ¼ that of the average thickness.

In our previous studies of SPIONs surfaces [29–32], we determined the elemental compositions of SPIONs, identifying issues that might affect the functionalization of SPIONs, their biological properties, etc. Here, we use highly surface-sensitive X-ray photoelectron spectroscopy (XPS) and time-of-flight secondary ion mass spectroscopy (TOF-SIMS) to study the NO functionalization of DMSA- and PEGdithiol-coated SPIONs, carried out under both nitrogen and oxygen atmospheres, and demonstrate the capabilities of these techniques to identify S—NO bond formation.

2. Materials and methods

All experiments were replicated five times.

2.1. SPION synthesis

Bare SPIONs, prepared by alkaline precipitation, as previously described [33], were treated with TEPSA [3-(triethoxysilyl) propyl succinic anhydride] in organic medium. Briefly, TEPSA (25 mmol; 7.1 mL)

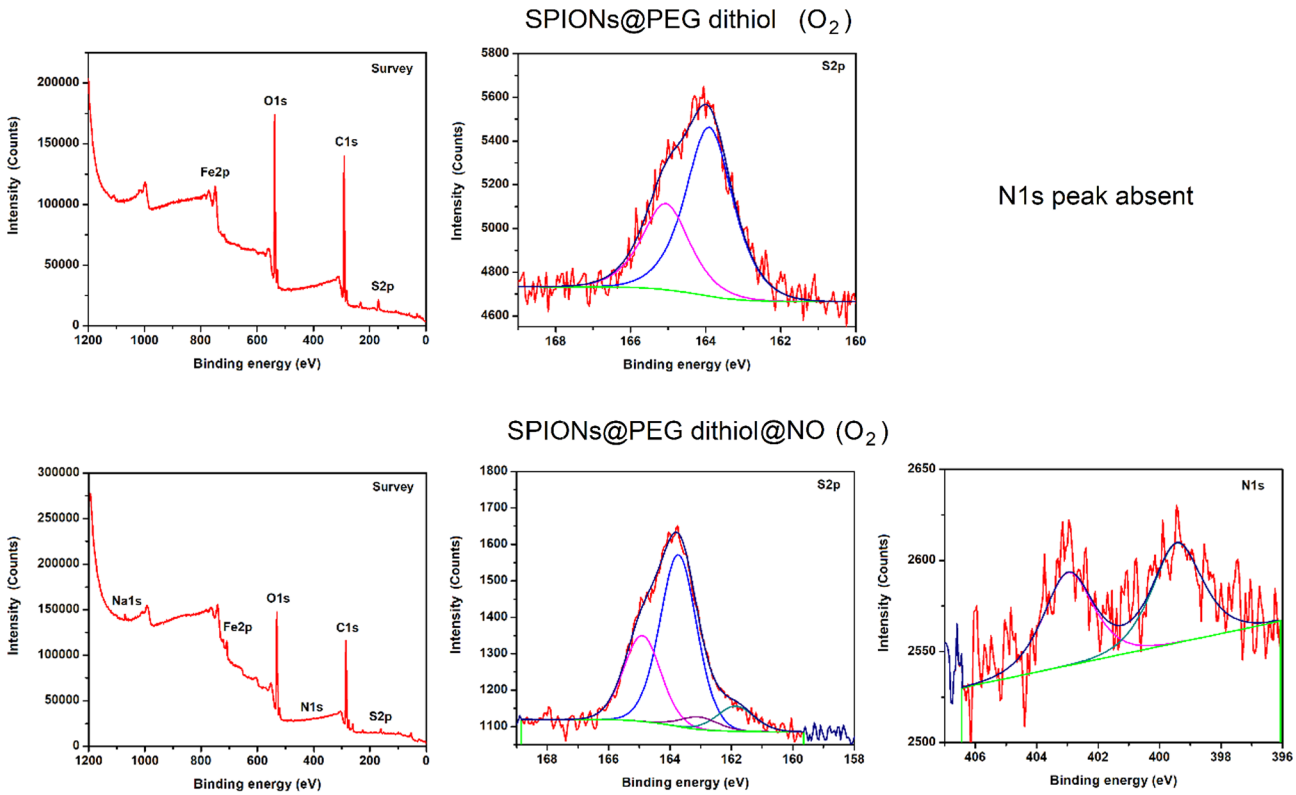

Fig. 3. XPS peaks of SPION@PEGdithiol (upper series) and SPION@PEGdithiol@NO (lower series).

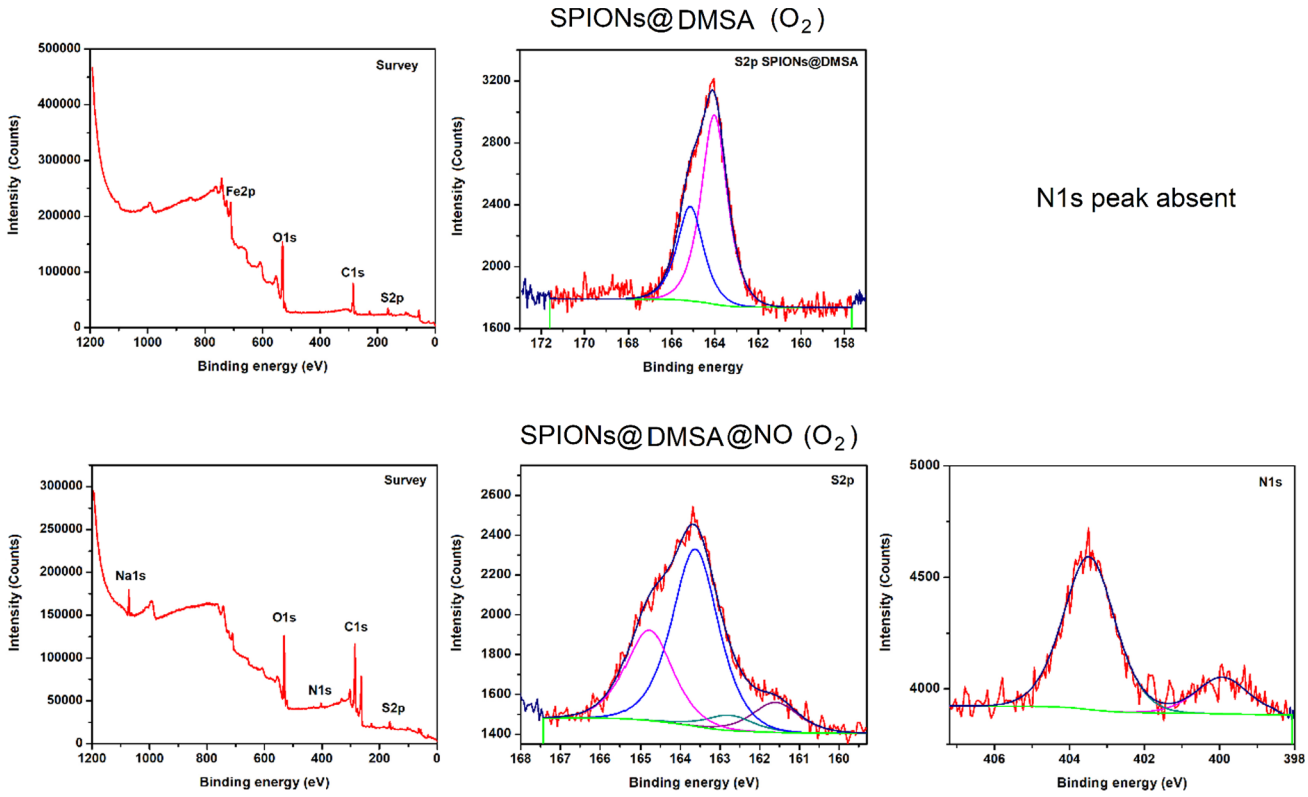

Fig. 4. XPS peaks of SPION@DMSA (upper series), and SPION@DMSA@NO (lower series).

was slowly added to a suspension of SPIONs in dimethyl formamide (50 mL; [Fe] = 100 mM). Water was added (4.3 mL), followed by an aqueous solution of tetramethylammonium hydroxide (2.5 mL; 1 M = 2.5 mmol) at room temperature, under stirring. The solution was heated at 100 °C for 24 h under continuous stirring. The SPIONs were collected by pouring the suspension into an acetone/diethyl ether mixture, followed by magnetic decantation. After washing with acetone, the black precipitate was dispersed in water and purified by

Table 1
XPS peak attributions of functionalized SPIONs.

XPS characterizations of PEGdithiol and DMSA functionalizations				
Attribution	PEGdithiol		DMSA	
	SPION@PEGdithiol (eV)	SPION@PEGdithiol-NO (eV)	SPION@DMSA (eV)	SPION@DMSA-NO (eV)
NH_2		399.4 (0.2 at%)		399.8 (0.4 at%)
SNO		403.0 (0.3 at%)		403.4 (1.8 at)
Fe—S		161.9 (0.3 at%)		161.5 (0.4 at%)
SH, S—S, S—N	163.9 (1.7 at%)	163.7 (1.0 at%)	164.0 (3.3 at%)	163.8 (2.1 at)

membrane filtration (membrane cut-off: 30 kDa) before centrifuging (16,500*g*; 45 min).

2.2. Thiolation

2.2.1. DMSA coating

One hundred mg of DMSA were dissolved in 5 mL of ethanol and mixed, under magnetic stirring at room temperature, with 1 mL of previously prepared SPIONs and 5 mL of milli-q water. The reaction time was 24 h, under either an oxygen or a nitrogen atmosphere; both gases were 99.99999% pure.

2.2.2. Pegdithiol coating

Five mg of PEG dithiol (M_n = 1000) were dissolved in 10 mL of milli-q water, using magnetic stirring at room temperature, with 1 mL of previously prepared SPIONs and 2 mL of milli-q water. The reaction time was 4 h under either an oxygen or a nitrogen atmosphere.

2.3. Nitrosation

Two mL of 60 mM $NaNO_2$ were added to the thiolated nanoparticles and mixed under magnetic stirring, at room temperature, for 3 h under either an oxygen or a nitrogen atmosphere. The solutions were centrifugated and filtrated three times, to remove contaminants.

2.4. Physicochemical characterizations

2.4.1. TEM

The samples were diluted in water and sonicated for 3 min to disperse the SPIONs. One drop of each sample was spread on a copper grid with a lacey carbon film, and analyzed on drying. The samples were bright-field imaged by transmission electron microscopy (TEM), using a JEM-2100F field emission electron microscope, with ultrahigh resolution, at a beam energy of 200 kV.

2.4.2. FTIR

IR spectra were obtained, in the range 450–4000 cm^{-1}, using a Bruker Alpha spectrometer, at a resolution of 4 cm^{-1}; 64 scans were coadded to improve S/N. The samples were deposited by placing several drops on a silicon substrate; ATR spectra were obtained using a diamond plate.

2.4.3. XPS

XPS was performed with a VG ESCALAB 3 MK II (Thermo VG Scientific), using non-monochromated Mg Kα X-rays (hν = 1253.6 eV). The instrument resolution was 0.7 eV, and a perpendicular take-off angle was used. The analysis chamber pressure was < 10^{-9} torr. After Shirley background removal, the component peaks were separated by the VG Avantage software. The energy was calibrated by setting the C1s C—C peak, to 285 eV. FWHM values were those previously established in our laboratory. The depths probed by this technique, for elements of present interest, range from 3 to 5 nm and, with proper peak intensity sensitivity factors, the relative atomic percentages determined are highly quantitative (± 5%).

2.4.4. TOF-SIMS

TOF-SIMS was carried out on an ION-TOF TOF-SIMS IV mass spectrometer, using a mono-isotopic Bi^+ beam, generated by a liquid metal gun mounted on the instrument. The beam current was 1.5 pA. Drops of the samples were deposited onto a silicon substrate, covering an area greater than 2 mm × 2 mm, and permitted to dry. Positive and negative ion spectra were calibrated using H^+, C^+, $C_xH_y^+$ (x = 1–5 and y = 1–12) and H^-, C^-, $C_xH_y^-$ (x = 1–5 and y = 1–12) peaks. The depths probed by this technique range from 1 to 1.5 nm but the peak intensities are qualitative.

3. Results

3.1. Thiolation and nitrosation under an oxygen atmosphere

3.1.1. Transmission electron microscopy

TEM images of bare SPIONs (Figs. 1a and 2a), ~10 nm in diameter, may be compared with nanoparticles functionalized with PEGdithiol (SPIONs@PEGdithiol, Fig. 1b and 1c) and DMSA (SPIONs@DMSA, Fig. 2b and 2c); the PEGdithiol layer is seen to have an average thickness of 2.7 ± 1.3 nm (Fig. 1e), while that of the DMSA is 3.1 ± 1.7 nm (Fig. 2e). In the case of PEGdithiol, the PEG chain is ~3× that of the thickness, indicating that the chains lie parallel to the SPION surface, as suggested by Fig. 1c; in the case of DMSA, the molecular length is ~¼ that of the thickness, indicating chain extension, as suggested by Fig. 2c.

3.1.2. X-Ray photoelectron spectroscopy

3.1.2.1. Thiolation. The survey spectra of SPION@PEGdithiol (Fig. 3, upper series) and SPION@DMSA (Fig. 4, upper series) reveal the presence of $S2p_{3/2}$, C1s, O1s and $Fe2p_{3/2}$ spectra. The $S2p_{3/2}$ peak, which we shall discuss, was found at ~164.0 eV in both series, and is attributed to the presence of SH and SS.

3.1.2.2. Nitrosation. It is known that some reactions carried out under an O_2 atmosphere generate S—S bonds [34], which, in the present case, would preclude the successful attachment of NO. For both SPION@PEGdithiol-NO and SPION@DMSA-NO, nitrosation produces a N1s spectrum (lower series of Figs. 3 and 4). The peaks, and their attributions, are found in Table 1. Subsequent to nitrosation, an additional shoulder appears in the $S2p_{3/2}$ spectrum, at ~161.5 eV, attributed to Fe—S; the $S2p_{3/2}$ peak at ~164 eV, which persists, may also be attributable to the formation of SN, seen in the N1s spectrum at 403 eV (0.3 at%) for SPION@PEGdithiol-NO and 403.4 eV (1.8 at%) for SPION@DMSA-NO. The N1s spectrum also contains a peak found at ~399.8 eV, attributed to amine, apparently generated as a byproduct during nitrosation. These peak attributions will be confirmed by the TOF-SIMS results presented below.

3.1.3. Time-of-Flight secondary ion mass spectrometry

3.1.3.1. Thiolation. The TOF-SIMs spectra of SPION@PEGdithiol (Fig. 5) and SPION@DMSA (Fig. 6) both indicate the presence of SH,

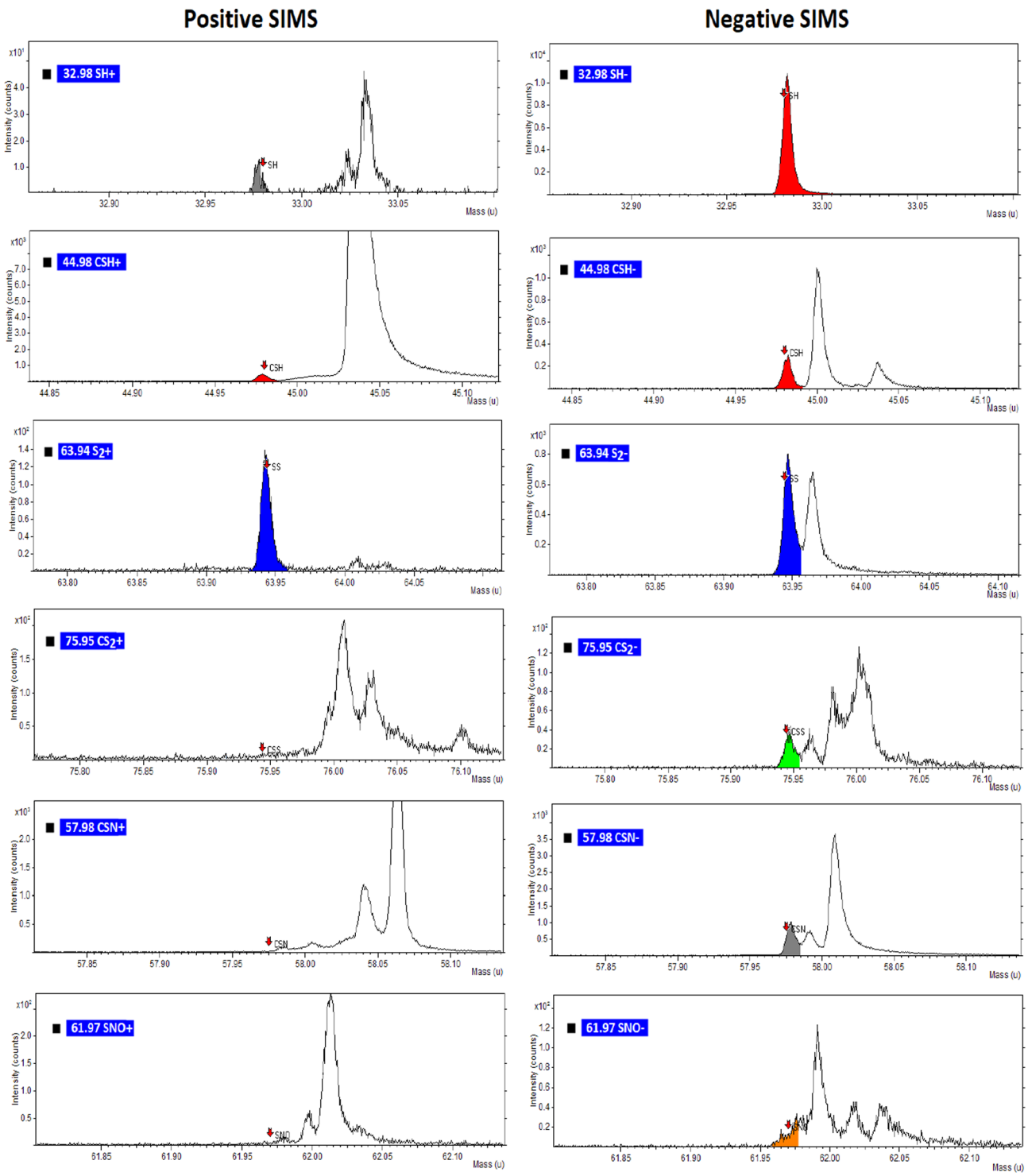

Fig. 5. TOF-SIMS HR spectra of SPION@PEGdithiol under oxygen atmosphere.

showing peaks at both 32.98 Da (SH) and 44.98 Da (C-SH), as well as peaks at both 63.94 Da (SS) and 75.95 Da (C-SS), confirming the XPS attributions of thiols and disulfides.

3.1.3.2. Nitrosation. On nitrosation, both SPION@PEGdithiol-NO (Fig. 7) and SPION@DMSA-NO (Fig. 8) still display peaks at 32.98 Da (SH) and 44.98 Da (C-SH), and at 63.94 Da (SS) and 75.95 Da (C-SS), indicating that not all the thiols groups underwent nitrosation. However, the successful nitrosation of some thiol groups was shown by peaks at 57.98 Da (C-SN) and 61.97 Da (SN—O), again supporting the XPS attributions.

3.1.4. FTIR spectroscopy

FTIR (Fig. 9) was used to determine spectral differences before and after nitrosation. The S—H stretch, expected at 2500–2600 cm^{-1}, was not displayed in any of the spectra. This is probably due to both the low extinction coefficient of the peak and the low concentration of S—H. In a similar fashion, neither S—NO (700–750 cm^{-1}) nor N—O (1320–1360 cm^{-1}) were in evidence, probably for the same reasons.

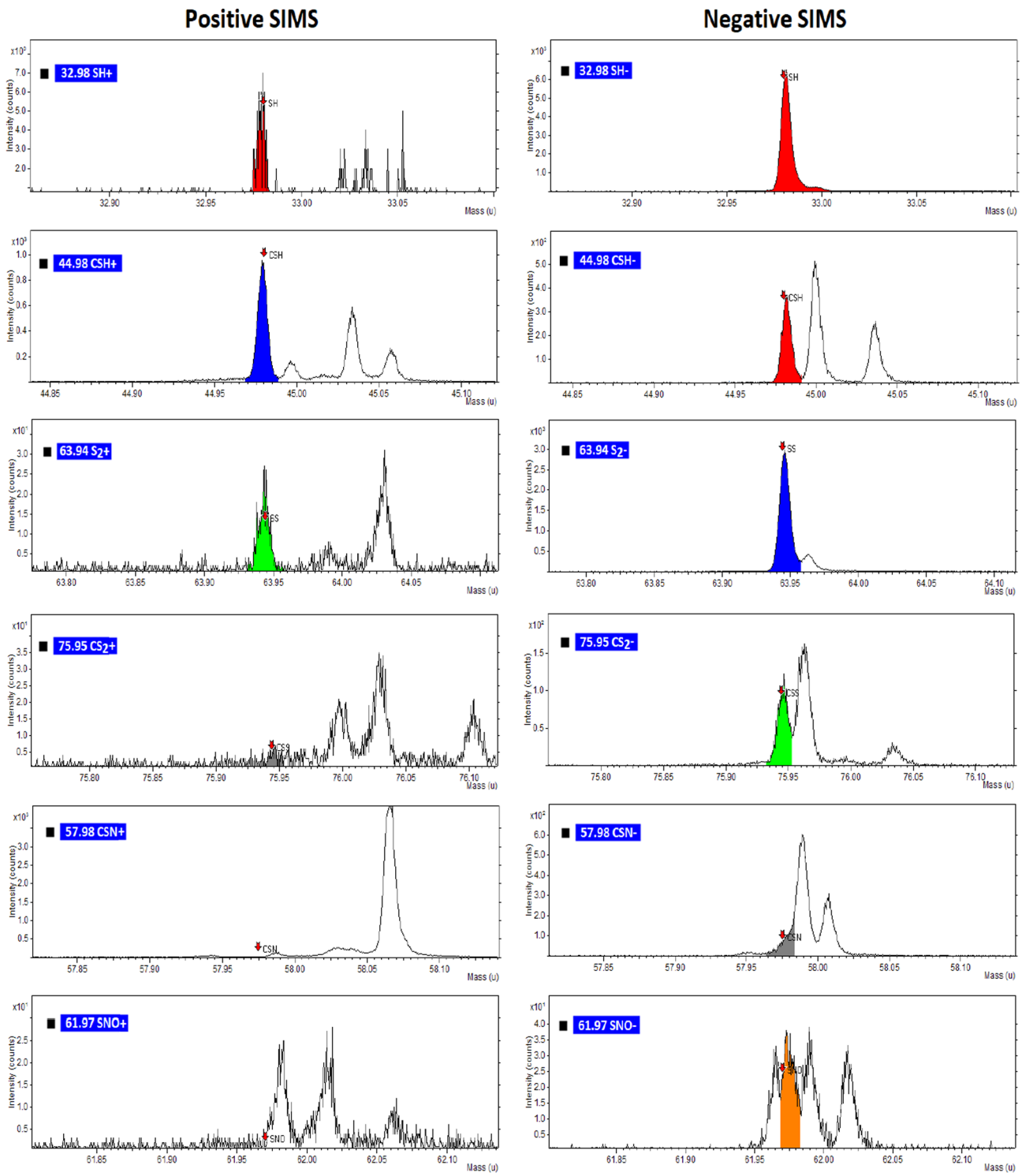

Fig. 6. TOF-SIMS HR spectra of SPIONs@DMSA under oxygen atmosphere.

3.2. Thiolation and nitrosation under a nitrogen atmosphere

3.2.1. XPS

3.2.1.1. Thiolation. The XPS spectra of SPIONs@PEGdithiol (Fig. 10) shows S2p$_{3/2}$ peaks at 163.7 and 167.8 eV, attributed to SH and SO_3, respectively. N1s peaks appear, even when nitrosation was not carried out, at 399.0 (NH), 400.2 (NH_2) and 407 eV (NO_3), indicating an unexpected reaction with the nitrogen atmosphere, since the subsequent use of an oxygen atmosphere gave no hint of glassware contamination. Similarly, SPIONs@DMSA (Fig. 11) shows free thiol at 164.2 (S—H), and unexpected N1s peaks at 402.0 and 403.1 eV. Clearly, the species introduced by the presence of a nitrogen atmosphere are reactive, subsequently oxidizing on exposure to air.

3.2.1.2. Nitrosation. Subsequent to SPIONs@PEG dithiol-NO nitrosation (Fig. 10, lower series), oxidation has increased, as

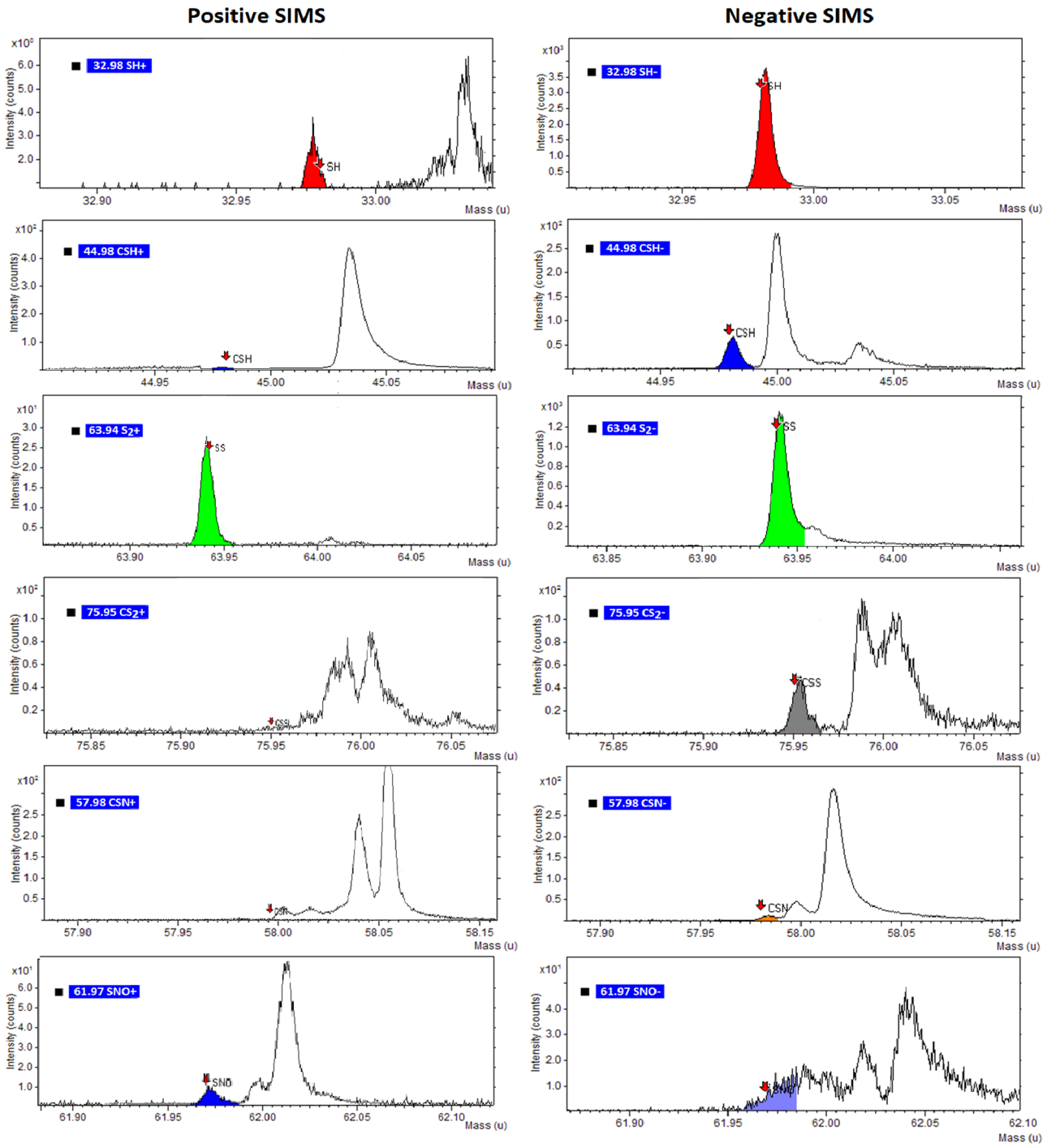

Fig. 7. TOF-SIMS HR spectra of SPION@PEGdithiol@NO under oxygen atmosphere.

evidenced by peaks at 168.6 eV (SO_4), 403.8 eV (NO_2) and 407.6 eV (NO_3), found in Table 2. On SPIONs@DMSA-NO nitrosation, the thiol peak at 163.7 eV remains and a new peak appears at 403.9 eV, attributed to SNO_2; the absence of a peak attributable to SNO indicates its oxidation. XPS attributions are found in Table 2.

3.2.2. TOF-SIMS

3.2.2.1. Thiolation. Figs. 12 and 13 indicate the presence of SH (39.98 Da), C-SH (48.98 Da) and C-SS (63.94 Da) for both series.

3.2.2.2. Nitrosation. The PEGdithiol series (Fig. 14) does not exhibit either C-SN or SN-O peaks, while the DMSA series (Fig. 15) exhibits a broad peak at the 61.97 Da position of SN-O. The appearance of SN-O_2 (77.96 Da) indicates that oxidation has occurred in both series

4. Discussion

4.1. Thiolation and nitrosation under an oxygen atmosphere

The TEM images in Figs. 1 and 2 display the successful formation of

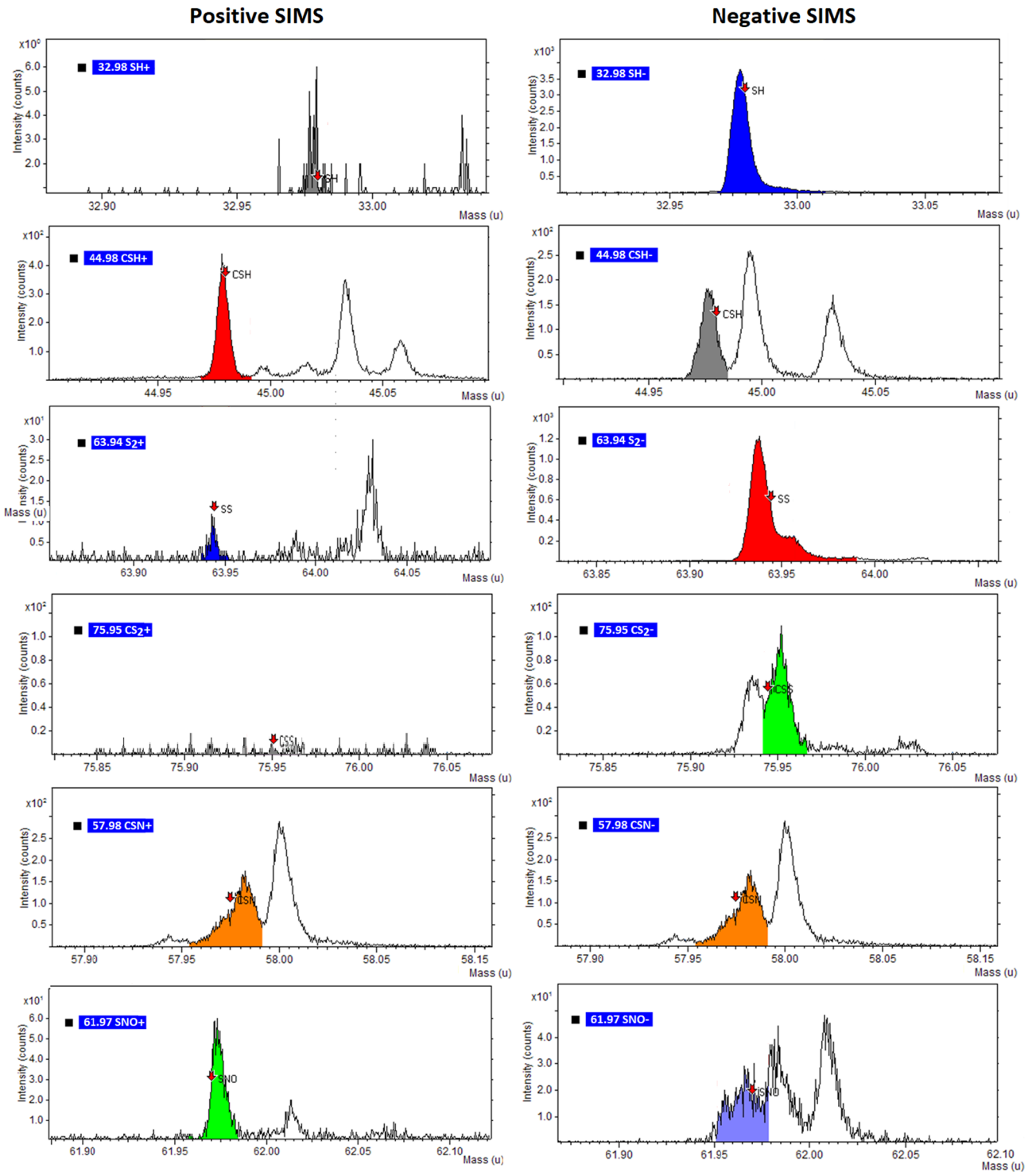

Fig. 8. TOF-SIMS HR spectra of SPION@DMSA@NO under oxygen atmosphere.

PEGdithiol and DMSA coatings around the nanoparticles, with the size distribution histograms showing large thickness variations for both systems. This indicates that the layers formed are not uniform, and that certain points might be free of functionalization, exposing the core nanoparticle.

XPS characterizations of both series (Figs. 3 and 4), before nitrosation, show the presence of free -SH groups, indicating both successful SH functionalization and the presence of S—S bonds. On nitrosation, the N1s spectra (Fig. 3, lower series) shows a shoulder on the $S2p_{3/2}$ peak, attributed to Fe—S, which may additionally be have a contribution from the presence of contaminant S—Na, detected by TOF-SIMS. The presence of a peak attributed to SNO (403 eV) indicates that an oxygen atmosphere contributes to NO attachment but cannot avoid secondary reactions, such as the formation of amine groups. Fig. 16

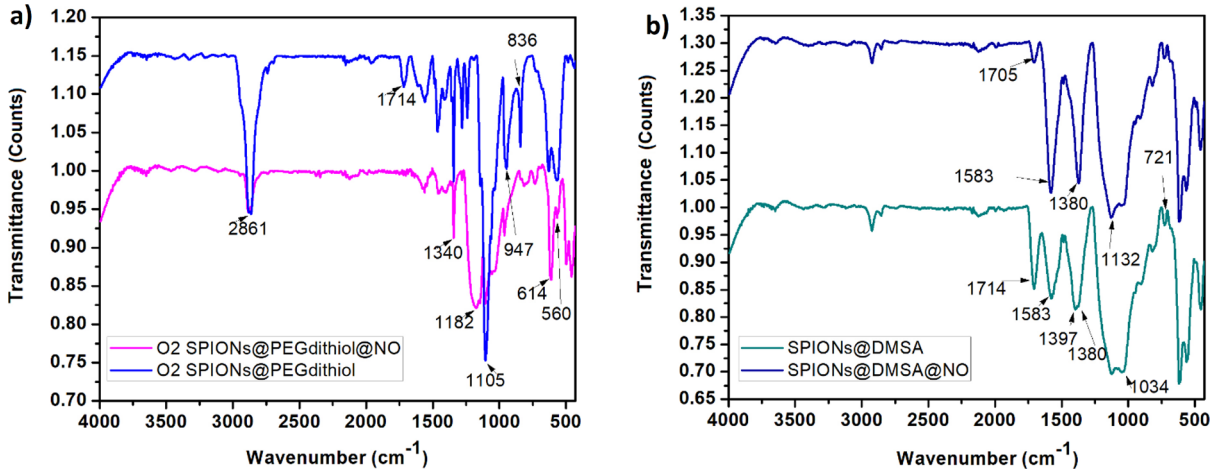

Fig. 9. FTIR spectral comparisons of a) SPION@PEGdithiol and SPION@PEGdithiol@NO and b) SPION@DMSA and SPION@DMSA@NO.

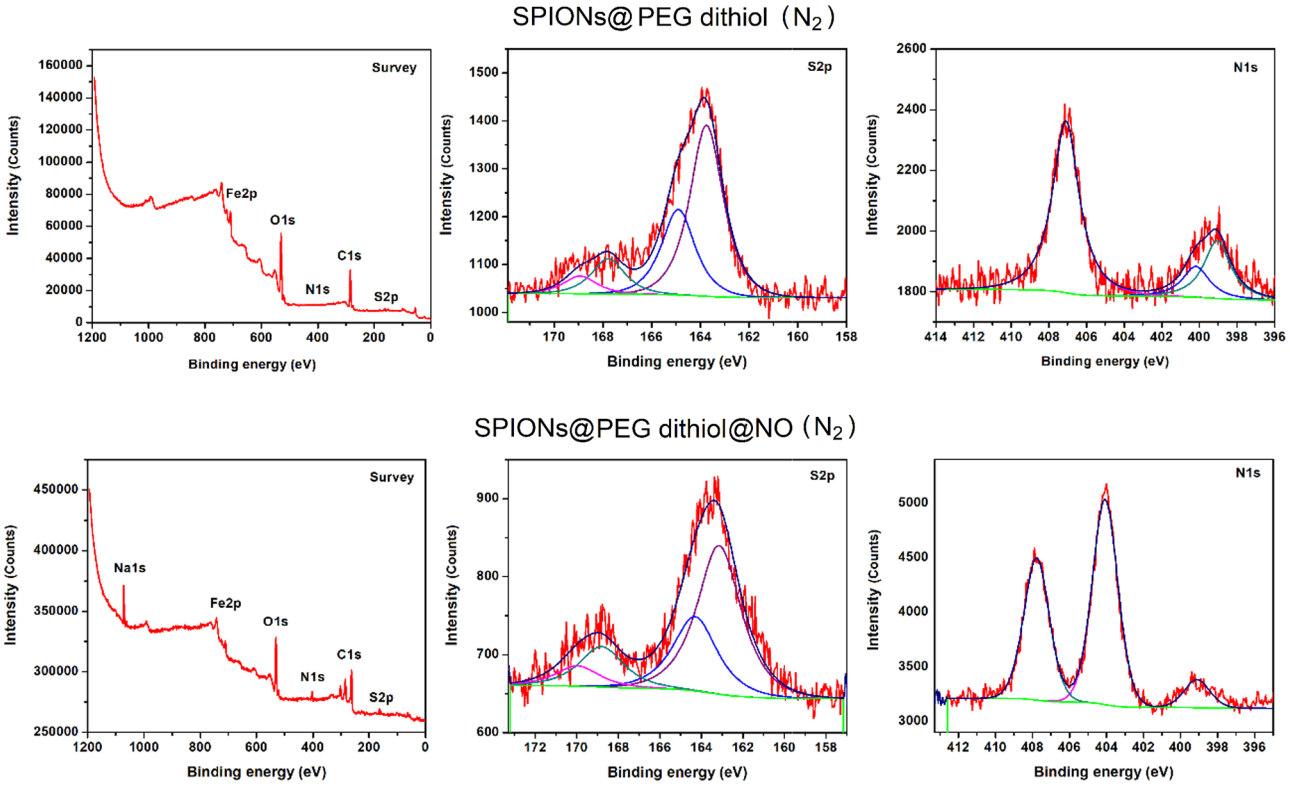

Fig. 10. XPS peaks of SPION@PEGdithiol (upper series) and SPION@PEGdithiol@NO (lower series) under a nitrogen atmosphere.

shows the XPS peak fittings used in this study; the actual Fe2p and C1s component peaks and attributions of the SPIONs used here are found in our previous article [27], which concerns their surface analysis.

TOF-SIMS supports the identification of SNO. Nitrosation was carried out several times, and only the oxygen atmosphere was able to produce the successful attachment of NO (Figs. 12 and 13).

Because of low peak extinction coefficients and low concentrations, FTIR is not an appropriate characterization tool in the present case.

4.2. Thiolation and nitrosation under a nitrogen atmosphere

When carried out under a nitrogen atmosphere, both series (Figs. 10 and 11) indicate the unexpected appearance of a N1s spectrum prior to nitrosation, as well as the oxidation of any SNO that was formed, to SNO_2.

The SNO peak is not displayed in the PEGdithiol TOF-SIMS spectrum (Fig. 12); however, it appears (61.97 Da) in the SPIONs@DMSA-NO spectrum, as does the SNO_2 peak (77.96 Da, Fig. 15), particularly intense in the negative SIMS spectrum. The presence of the SNO peak in SPIONs@DMSA-NO spectrum implies that some attachment of NO occurred, which was subsequently oxidized to SNO_2. Although we are unable to distinguish among S—H, S—S and S—N (see Table 1) because they all have an XPS peak at the same energy, we can estimate a minimum value for SNO formation by assuming that the S—H contribution to the (S—H + S—S + S—N) composite peak is 100%. As seen for SPION@PEGdithiol-NO (Table 1), the minimum value corresponds

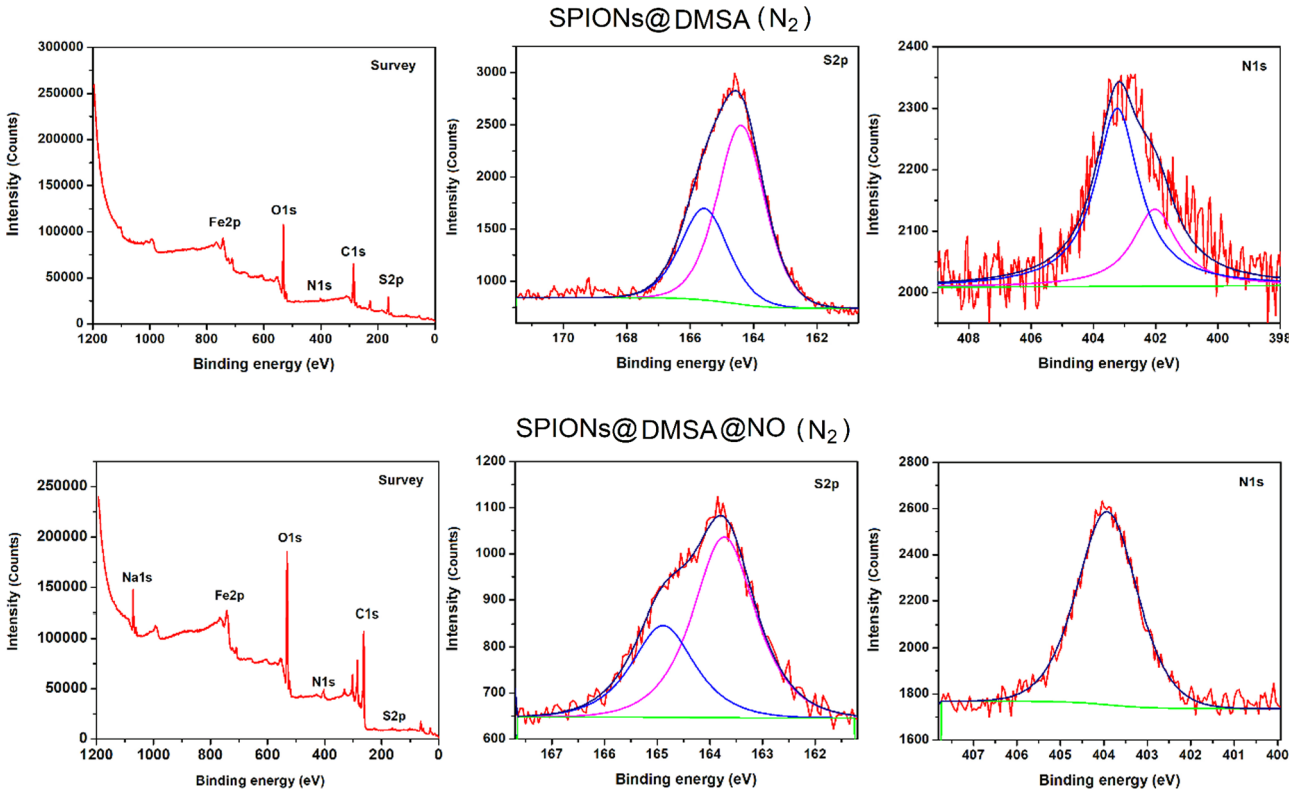

Fig. 11. XPS peaks of SPION@DMSA (upper series) and SPION@DMSA@NO (lower series) under a nitrogen atmosphere.

Table 2
XPS peak attributions of functionalized SPIONs under a nitrogen atmosphere.

Comparison of PEGdithiol and DMSA XPS characterization				
Suggested Attribution	PEG dithiol		DMSA	
	SPION@PEGdithiol (eV)	SPION@PEGdithiol-NO (eV)	SPION@DMSA (eV)	SPION@DMSA-NO (eV)
SH, S–S	163.7 (1.2 at%)	163.5 (0.4 at%)	164.2 (7.2 at%)	163.7 (2.0 at%)
SO_3^{2-}	167.8 (0.2 at%)			
SO_4^{2-}		168.6 (0.2 at%)		
=C–NH	399.0 (0.7 at%)	399.1 (0.6 at%)		
C–NH_2	400.2 (0.4 at%)			
C–NH_n^+			402.0 (0.6 at%)	
NO			403.1 (1.5 at%)	
NO_2, SNO_2		403.8 (4.8 at%)		403.9 (4.7 at%)
NO_3	407.0 (2.0 at%)	407.6 (4.2 at%)		

to 0.3/1.0 = 30%; for SPION@DMSA-NO, the minimum value corresponds to 1.8/2.1 = 86%.

4.3. Generalities and comparisons of the NO attachment processes under oxygen and nitrogen atmospheres

The results of the two series, carried out under both oxygen and nitrogen atmospheres, are found in Table 3. The most surprising results pertain to the influences of the atmospheres under which the reactions occurred: nitrosation (SNO) is achieved only under an oxygen atmosphere, while the nitrogen atmosphere proves unexpectedly reactive, introducing N-containing species that, on subsequent exposure to air, oxidize to SNO_2.

5. Conclusions

We show the successful attachment of NO to SPIONs for reactions occurring under an oxygen atmosphere, but not under a nitrogen atmosphere. In the latter case, the atmosphere influences the reaction, introducing species that ultimately oxidize on exposure to atmosphere.

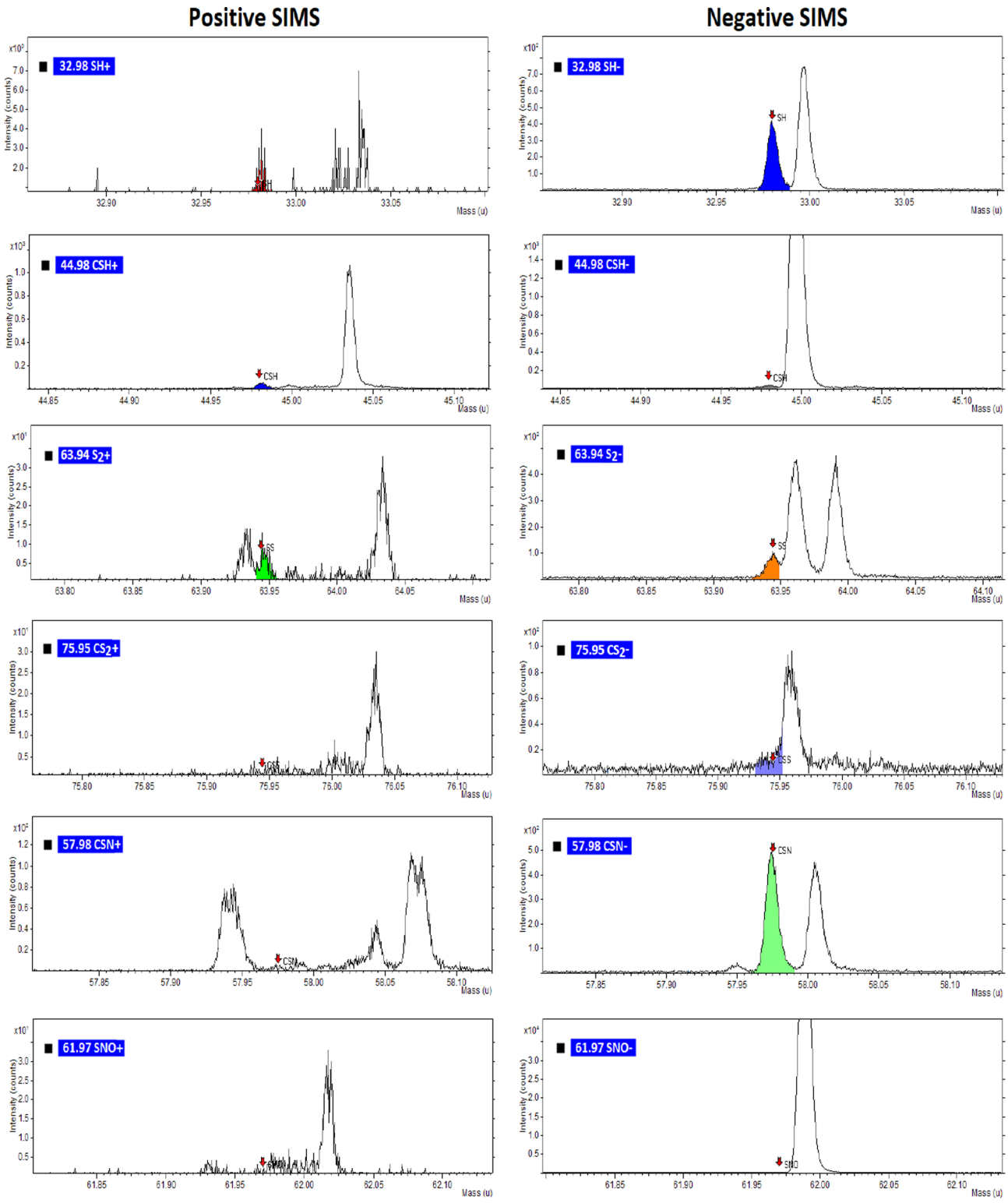

Fig. 12. ToF-SIMS HR spectra of SPION@PEG dithiol under nitrogen atmosphere.

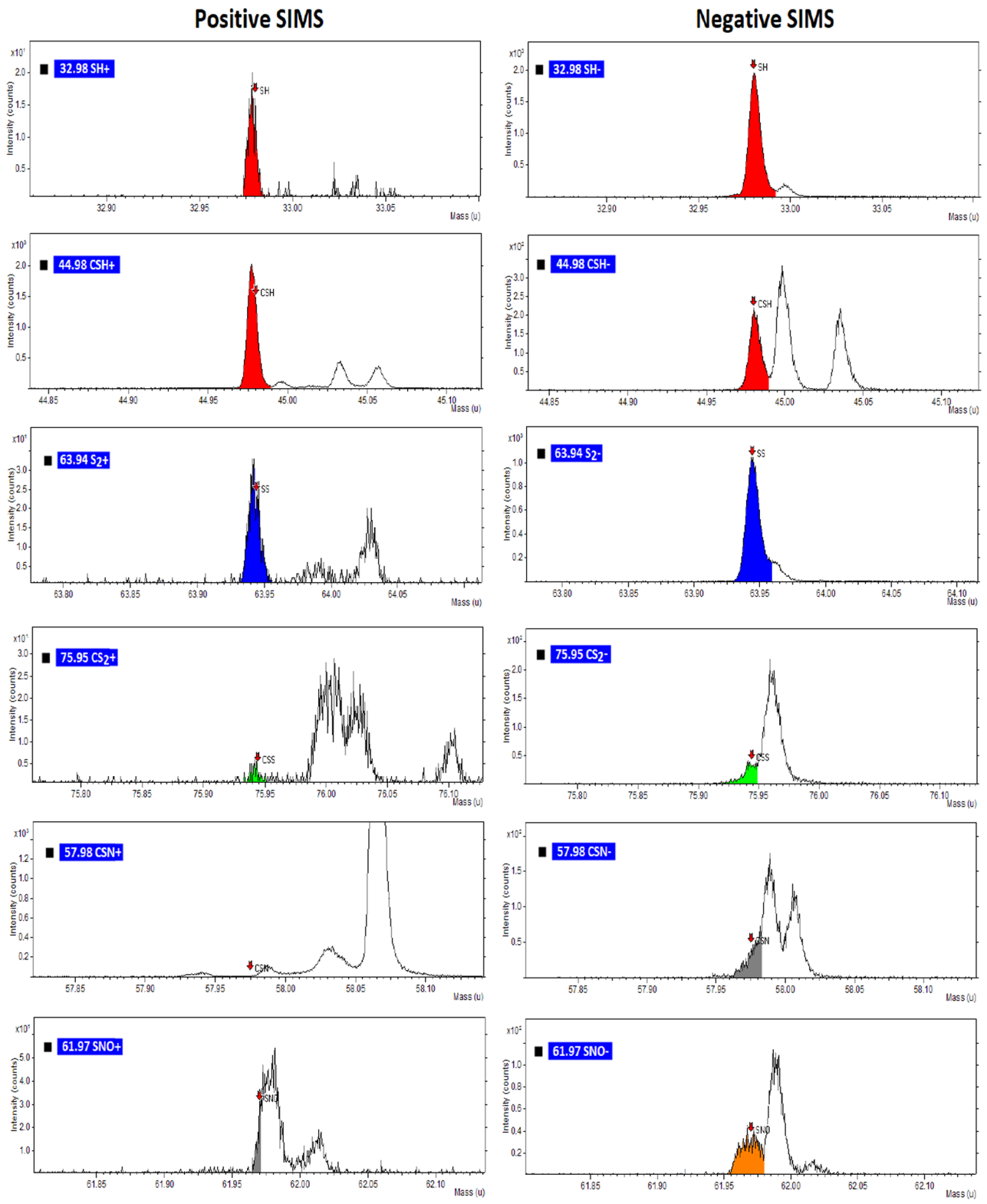

Fig. 13. TOF-SIMS HR spectra of SPION@DMSA under a nitrogen atmosphere.

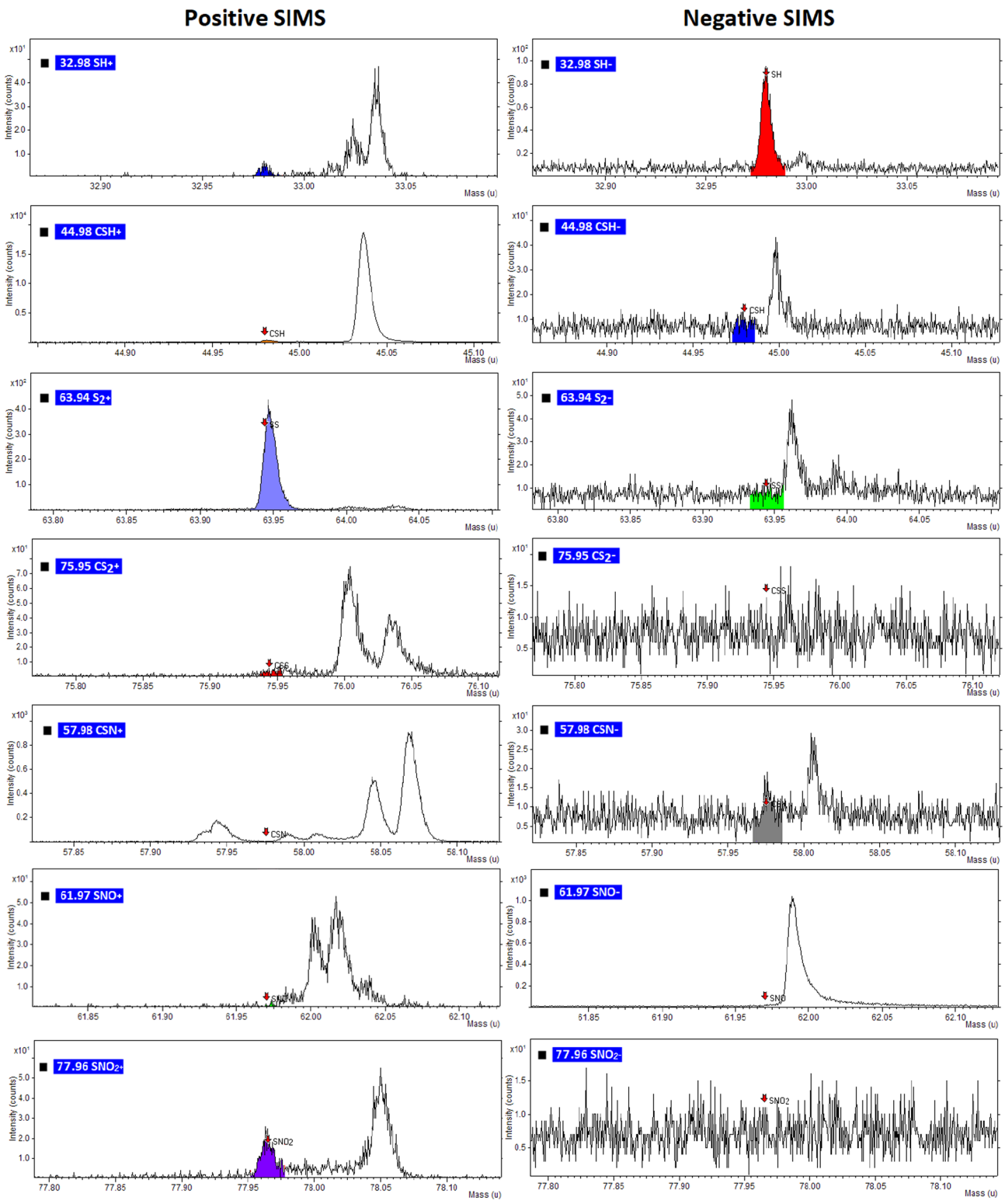

Fig. 14. TOF-SIMS HR spectra of SPION@PEGdithiol@NO under a nitrogen atmosphere.

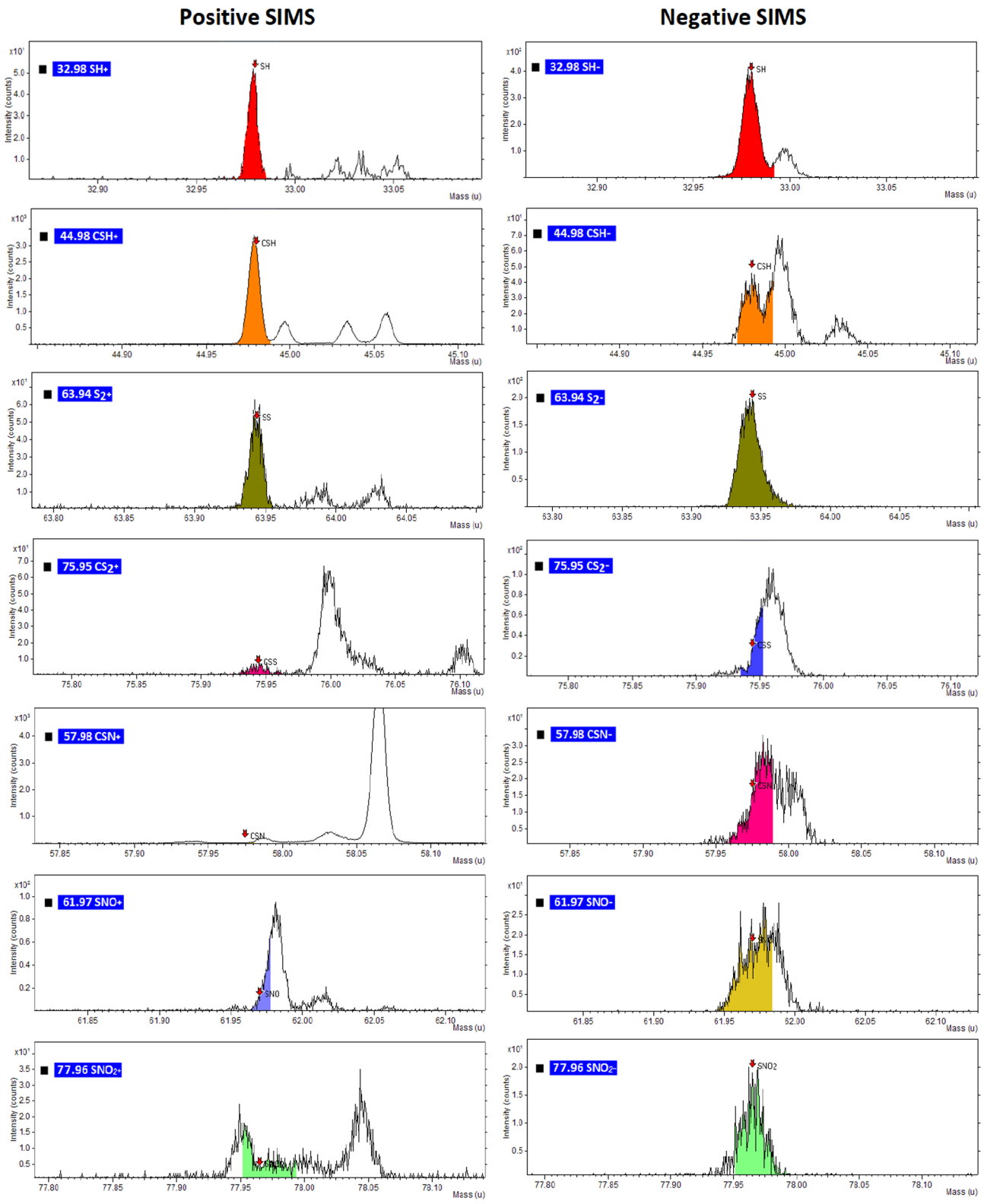

Fig. 15. TOF-SIMS HR spectra of SPION@DMSA@NO under a nitrogen atmosphere.

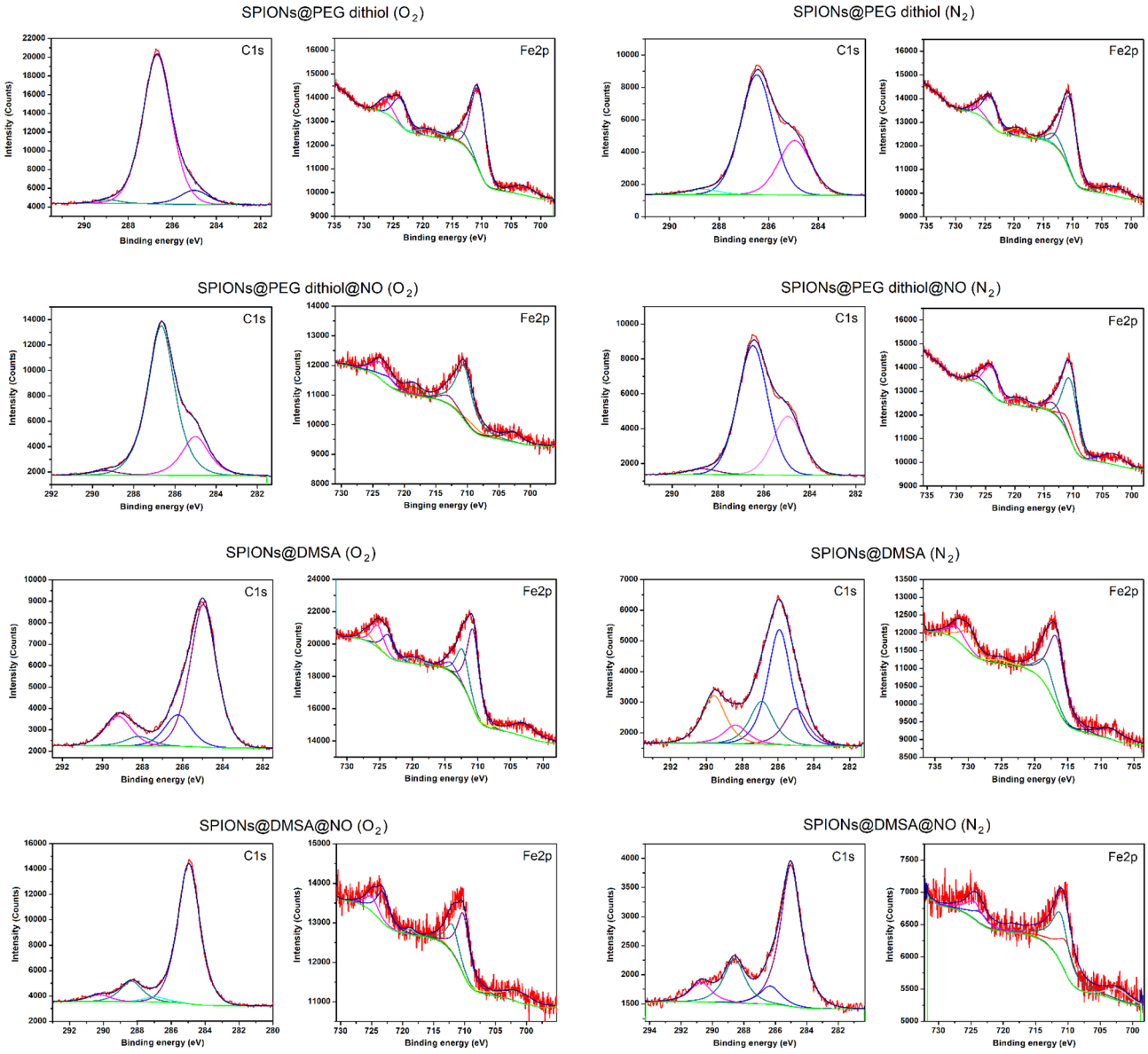

Fig. 16. XPS peak fitting of C1s and Fe2p spectra.

Table 3
A comparison of influences of oxygen and nitrogen atmospheres.

O_2 atmosphere	N_2 atmosphere
–	N1s appear on thiolation (unexpected)
N1s appear on nitrosation	N1s appear on nitrosation
S—S bonds appear	S—S bonds appear
Fe—S peak found on SPIONs@PEGdithiol@NO	Fe—S peak found on SPIONs@PEGdithiol@NO
Fe—S peak found on SPIONs@DMSA@NO	–
amine group found on SPIONs@PEGdithiol-NO	Amine group found on SPIONs@PEGdithiol-NO
amine group found on SPIONs@DMSA-NO	–
S—NO bond	S—NO_2 group
–	Oxidation of $S2p_{3/2}$ and N1s

Credit authorship contribution statement

L.K. Mireles: Investigation, Methodology, Conceptualization, Writing - original draft. **D. Stanicki:** Validation. **S. Laurent:** Supervision, Validation. **D. Deschênes:** Validation. **E. Sacher:** Validation, Writing - review & editing, Supervision. **L'H. Yahia:** Visualization, Supervision.

Declaration of Competing Interest

The authors declare that they have no known competing financial interests or personal relationships that could have appeared to influence the work reported in this paper.

Acknowledgements

This work was supported by the Fonds de recherche du Québec, the Natural Sciences and Engineering Research Council of Canada (NSERC) and the Groupe de recherche en sciences et technologies biomédicales (GRSTB). It was also supported by the Fond National de la Recherche Scientifique (FNRS), UIAP VII, ARC Programs of the French Community of Belgium, COST Actions and the Walloon region (Gadolymph and Holocancer programs). We thank Josianne Lefebvre for assistance in processing the XPS and TOF-SIMs data, and Rafaella Oliveira do Nascimento for contributions during discussions.

References

[1] J. MacMicking, Q.W. Xie, C. Nathan, Nitric oxide and macrophage function, Annu. Rev. Immunol. 15 (1997) 323–350.
[2] R.L. Mancinelli, C.P. McKay, Effects of nitric oxide and nitrogen dioxide on bacterial growth, Appl. Environ. Microbiol. 46 (1) (1983) 198–202.
[3] R.P. Howlin, K. Cathie, L. Hall-Stoodley, V. Cornelius, C. Duignan, R.N. Allan, B.O. Fernandez, N. Barraud, K.D. Bruce, J. Jefferies, M. Kelso, S. Kjelleberg, S.A. Rice, G.B. Rogers, S. Pink, C. Smith, P.S. Sukhtankar, R. Salib, J.S. Webb, Low-Dose Nitric Oxide as Targeted Anti-biofilm Adjunctive Therapy to Treat Chronic *Pseudomonas aeruginos*a Infection in Cystic Fibrosis, Mol. Ther. 25 (9) (2017) 2104–2116.
[4] A. Friedman, J. Friedman, New biomaterials for the sustained release of nitric oxide: past, present and future, Exp. Opin. Drug. Del. 6 (10) (2009) 1113–1122.
[5] A.J. Gow, C.R. Farkouh, D.A. Munson, M.A. Posencheg, H. Ischiropoulos, Biological significance of nitric oxide- mediated protein modifications, Am. J. Physiol. Lung Cell Moll. Physiol. 287 (2004) L262–L268.
[6] B.J. Nablo, H.L. Prichard, R.D. Butler, B. Klitzman, M.H. Schoenfisch, Inhibition of implant associated infections via nitric oxide release, Biomaterials 26 (34) (2005) 6984–6990.
[7] A. Trampuz, A.F. Widmerm, Infections associated with orthopedic implants, Clin. Infect. Dis. 2 (33) (2001) S94.
[8] M. Wilcox, P. Kite, K. Mills, S. Sugden, In situ measurement of linezolid and vancomycin concentrations in intravascular catheter-associated biofilm, J. Antimicrob. Chemother. 47 (2001) 171–175.
[9] C. Jardeleza, B. Thierry, S. Rao, S. Rajiv, A. Drilling, D. Miljkovic, S. Paramasivan, C. James, D. Dong, N. Thomas, S. Vreugde, C.A. Prestidge, P.J. Wormald, An in vivo safety and efficacy demonstration of a topical liposomal nitric oxide donor treatment for Staphylococcus aureus biofilm–associated rhinosinusitis, Transl. Res. 166 (6) (2015) 683–692.
[10] G. Laverty, S.P. Gorman, B.F. Gilmore, Biomolecular mechanisms of Pseudomonas aeruginosa and Escherichia coli biofilm formation, Pathogens 3 (2014) 596–632.
[11] B.J. Privett, A.D. Broadnax, S.J. Bauman, D.A. Riccio, M.H. Schoenfisch, Examination of Bacterial Resistance to Exogenous Nitric Oxide, Nitric. Oxide. 26 (3) (2012) 169–173.
[12] J. Saraiva, S.S. Marotta-Oliveira, S.A. Cicillini, J.D.O. Eloy, J.M. Marchetti, Nanocarriers of nitric oxide delivery, J. Drug. Deliv. (2011) 936438.
[13] X. Zhang, S. Mansouri, D.A. Mbeh, L'H. Yahia, E. Sacher, T. Veres, Nitric oxide delivery by core/shell superparamagnetic nanoparticle vehicles with enhanced biocompatibility, Langmuir 28 (35) (2012) 12879–12885.
[14] B.V. Worley, K.M. Schilly, M.H. Schoenfisch, Anti-biofilm efficacy of dual-action nitric oxide-releasing alkyl chain modified poly(amidoamine) dendrimers, Mol. Pharm. 12 (2015) 1573–1583.
[15] A.J. Friedman, G. Han, M.S. Navati, M. Chacko, L. Gunther, A. Alfieri, J.M. Friedman, Sustained release nitric oxide releasing nanoparticles: charac- terization of a novel delivery platform based on nitrite containing hydrogel/glass composites, Nitric. Oxide 19 (2008) 12–20.
[16] F. Afkhami, S. Taherkhani, M. Mohammadi, S. Martel, Encapsulation of magnetotactic bacteria for targeted and controlled delivery of anticancer agents for tumor therapy, Conf Proc IEEE Eng Med Biol Soc. 2011, pp. 6668–6671.
[17] R.T. Liu, J. Liu, J.Q. Tong, T. Tang, W.C. Kong, X.W. Wang, Y. Li, J.T. Tang, Heating effect and biocompatibility of bacterial magnetosomes as potential materials used in magnetic fluid hyperthermia, Prog. Nat. Sci.- Mater. 22 (1) (2012) 31–39.
[18] D.A. Mbeh, R. França, Y. Merhi, X.F. Zhang, T. Veres, E. Sacher, L'.H. Yahia, In vitro biocompatibility assessment of functionalized magnetite nanoparticles: biological and cytotoxicological effects, J. Biomed. Mater. Res. A 100 (6) (2012) 1637–1646.
[19] D.A. Mbeh, L.K. Mireles, D. Stanicki, L. Tabet, K. Maghni, S. Laurent, E. Sacher, L'.H. Yahia, Human alveolar epithelial cell responses to core-shell superparamagnetic iron oxide nanoparticles (SPIONs), Langmuir 31 (2015) 3829–3839.
[20] A.K. Gupta, S. Wells, Surface-modified superparamagnetic nanoparticles for drug delivery: preparation, characterization, and cytotoxicity studies, IEEE. Trans. Nanobiosci. 3 (1) (2004) 66–73.
[21] C. Tassa, S.Y. Shaw, R. Weissleder, Dextran-coated iron oxide nanoparticles: a versatile platform for targeted molecular imaging, molecular diagnostics, and therapy, Acc. Chem. Res 44 (10) (2011) 842–852.
[22] Y.F. Li, C. Chen, Fate and toxicity of metallic and metal-containing nanoparticles for biomedical applications, Small 7 (2011) 2965–2980.
[23] R. Mejias, S. Perez-Yague, L. Gutierrez, L.I. Cabrera, R. Spada, P. Acedo, C.J. Serna, F.J. Lazaro, A. Villanueva, P. Morales Mdel, D.F. Barber, Dimercaptosuccinic acid-coated magnetite nanoparticles for magnetically guided in vivo delivery of interferon gamma for cancer immunotherapy, Biomaterials 32 (2011) 2938–2952.
[24] S. Naqvi, M. Samim, M. Abdin, F.J. Ahmed, A. Maitra, C. Prashant, A.K. Dinda, Concentration-dependent toxicity of iron oxide nanoparticles mediated by increased oxidative stress, Int. J. Nanomed. 5 (2010) 983–989.
[25] C.G. Gölander, J.N. Herron, K. Lim, P. Claesson, P. Stenius, J.D. Andrade, Properties of Immobilized PEG Films and the Interaction with Proteins, in: J.M. Harris (Ed.), Biotechnical and Biomedical Applications, Plenum, New York, 1992, pp. 221–245.
[26] A. Ruiz, P.C. Morais, R. Bentes de Azevedo, Z.G.M. Lacava, A. Villanueva, Morales M. Del Puerto, Magnetic nanoparticles coated with dimercaptosuccinic acid: development, characterization, and application in biomedicine, J. Nanopart. Res. 16 (2014) 2589.
[27] Y. Ikeda, Y. Nagasaki, PEGylation technology in nanomedicine, Adv. Polym. Sci. 247 (2011) 115–140.
[28] U. Wattendorf, H.P. Merkle, PEGylation as a tool for the biomedical engineering of surface modified microparticles, J. Pharm. Sci. 97 (2008) 4655–4669.
[29] L.K. Mireles, E. Sacher, L'.H. Yahia, S. Laurent, D. Stanicki, Acomparative physico chemical, morphological and magnetic study of silane-functionalized superparamagnetic iron oxide nanoparticles prepared by alkaline coprecipitation, Int. J. Biochem. Cell Biol. 75 (2016) 203–211.
[30] L.K. Mireles, E. Sacher, L.'H. Yahia, S. Laurent, D. Stanicki, Washing effect on superparamagnetic iron oxide nanoparticles, Data in Brief 7 (2016) 1296–1301.
[31] R. França, X.F. Zhang, T. Veres, L.'H. Yahia, E. Sacher, Core–shell nanoparticles as prodrugs: possible cytotoxicological and biomedical impacts of batch-to-batch inconsistencies, J. Colloid. Interface. Sci. 1 (389) (2013) 292–297.
[32] D.A. Mbeh, L.K. Mireles, D. Stanick, L. Tabet, K. Maghni, S. Laurent, E. Sacher, Yahia L'H. Human alveolar epithelial cell responses to core–shell superparamagnetic iron oxide nanoparticles (SPIONs), Langmuir. 31 (2015) 3829–3839.
[33] J.L. Bridot, D. Stanicki, S. Laurent, S. Boutry, Y. Gossuin, P. Leclère, R. Lazzaroni, L. Vander-Elst, R.N. Muller, New carboxysilane-coated iron oxide nanoparticles for nonspecific cell labelling, Contrast. Media. Mol. Imaging 8 (2013) 466–474.
[34] I.V. Koval, The chemistry of disulfides, Russ. Chem. Rev. 63 (9) (1994) 735–750.